Chinese Journal of
POLYMER SCIENCE

RESEARCH ARTICLE

https://doi.org/10.1007/s10118-026-3599-4
Chinese J. Polym. Sci.

Accelerating Field-based Simulations of Block Copolymers by Exploring Symmetry of Chain Architectures

Jun-Yang Liu, Yu-Chen Zhang, and Yi-Xin Liu*

State Key Laboratory of Molecule Engineering of Polymers, Department of Macromolecular Science, Fudan University, Shanghai 200433, China

Abstract Recent advances in polymer synthesis have enabled the creation of block copolymers with increasingly complex chain architectures, presenting exciting opportunities for novel materials design. However, elucidating and exploring their intricate mesophase behavior calls for highly efficient computational tools. Building upon recent developments in optimizing propagator computations for branched polymers, such as dynamic programming approaches and extensions of comb polymer methods, we introduce a novel topology-driven acceleration algorithm specifically designed for graph-enhanced field-based simulations (FBS) of block copolymers. Unlike prior methods focused on specific redundancies, our approach leverages graph isomorphism for topological decomposition, enabling systematic handling of symmetries in arbitrary architectures. Comprehensive benchmark tests on diverse complex architectures, including miktoarm star polymers and dendrimers, demonstrate significant computational speed-ups across a wide range of ordered phases. The acceleration algorithm not only enables rapid exploration of vast parameter spaces for complex block copolymer systems with self-consistent field theory (SCFT) simulations but also maintains full compatibility with sampling-based field-theoretical simulations (FTS), facilitating broader applicability in computational polymer science.

Keywords Block copolymers; Self-consistent field theory; Graph theory; Graph isomorphism

Citation: Liu, J. Y.; Zhang, Y. C.; Liu, Y. X. Accelerating field-based simulations of block copolymers by exploring symmetry of chain architectures. *Chinese J. Polym. Sci.* https://doi.org/10.1007/s10118-026-3599-4

INTRODUCTION

The ordered arrangement of soft matter into condensed structures with specific symmetries and spatial periodicity endows materials with exceptional properties, offering the potential to enhance current performance and allowing the development of entirely new applications.[1] Soft mesocrystals self-assembled by block copolymers with controllable feature sizes in mesoscale have effectively promoted the development of photonic crystals, catalyst scaffolds, microelectronic templates, and so on.[2–6] With the deepening of theoretical studies and the advancements in precise synthesis techniques, modern works focus on increasingly complex chain architectures such as miktoarm architectures and highly branched multiblock copolymers.[7–9] Recent advances in controlled polymerization techniques provide an effective platform for synthesizing block copolymers with precise architectures, bringing the range of experimental studies increasingly closer to the predicted parameter spaces made by theoretical studies. Kim *et al.* investigated the morphologies of the miktoarm star copolymer [PS_L-(PS_S-b-P_2VP)$_3$].[10] Dong *et al.* achieved precise control of the architectural evolution within a library of isomeric polymers (*i.e.*, 3AB $\longrightarrow$ 3(AB_1)B_2 $\longrightarrow$ 3(AB)) and stabilized the A15 and HEX phases at a higher volume fraction.[11] These results are consistent with predictions based on self-consistent field theory (SCFT).[12] Shi *et al.*[13] developed a monomer emulsified aqueous ring-opening metathesis polymerization for the highly efficient synthesis of star polymers with high molecular weight and arm conversion. Bates *et al.*[14] proposed a modular platform that allows for clean generation of A(BA′)$_n$ polymers with versatility in the selection of A and B chemistries.

Close collaboration between experimental and theoretical studies has significantly accelerated the exploration of novel phases using block copolymers.[4,14–17] With increasing experimental validation, field-based simulation (FBS) methods, including SCFT for mean-field saddle-point calculations and field-theoretic simulations (FTS) that account for field fluctuations, remain one of the most powerful approaches for predicting target phase regions and constructing required phase diagrams.[16,17] Among them, SCFT has been extensively used to access thermodynamic stability of a large number of ordered phases, demonstrating accurate predictive capability for intermediate to strong segregation regimes.[18] However, the rapid expansion of mesophases and the introduction of increasingly complex chain architectures have resulted in an exponentially growing parameter space to be explored, leading to an enormous increase in both the computational and human costs required for theoretical predictions. To promote research efficiency, established methods for SCFT operate through three levels: the base level methods focus on accelerating the solution of modified diffusion equations (MDE),

* Corresponding author, E-mail: lyx@fudan.edu.cn
Received December 16, 2025; Accepted January 28, 2026; Published online April 17, 2026

such as operator splitting (OS2),[19] RQM4,[20] ETDRK4[21] and crystallographic FFT algorithms;[22] the middle level methods aim to reduce the number of iterative steps, such as the Anderson mixing scheme; the top level methods try to minimize the number of evaluations of free energies in a fixed cell, such as the variable cell method to find the equilibrium cell size for unit cell calculations.[23] Accelerating FBS from the perspective of reducing the number of propagators to be evaluated, which usually corresponds to the most computationally expensive parts of FBS, is essentially orthogonal to existing acceleration methods. Leveraging topological symmetries inherent in chain architectures, the method with the core idea of reusing propagators can be developed, which is able to serve as a front-end enhancement to various existing numerical workflows to collaboratively improve computational efficiency.

In our previous work on fully automated chain architecture screening for ordered phases, online architectural modification was achieved through a graph-enhanced SCFT framework.[24] This generic graph representation enables online switching architectures without re-implementing SCFT algorithms and facilitates automated chain architecture screening for discovery of new stable phases. Building upon this formulation, the current study proposes an accelerated computational strategy by systematically optimizing the propagator evaluation sequence. Our method identifies propagator equivalence through topological decomposition and hierarchical analysis based on graph isomorphism, leading to a significant reduction in the number of propagators to be evaluated. Recently, two related works have appeared: Yong and Kim[25] presented a dynamic-programming scheme for acyclic branched polymers, while Li *et al.*[26] reported an aggregation-based approach for nested tree-like topologies in bottlebrush systems. Both studies achieve redundancy-free efficiency by systematically tabulating intermediate propagators. Rather than adopting either framework, our work introduces a distinct topology-driven strategy rooted in graph isomorphism, which systematically decomposes chains and identifies equivalent propagators hierarchically. This not only complements existing methods but also enhances automation in graph-enhanced FBS frameworks, enabling broader applicability to miktoarm, dendritic and other complicated chain architectures.

In this study, we provide a detailed implementation of the graph representation of block copolymers and use SCFT as the numerical backend to test its effectiveness. The implementation of the proposed algorithms is open-source and freely available at https://github.com/liuyxpp/PolymerArchitecture.jl. The results demonstrate that our method can efficiently handle arbitrary non-cyclic chain architectures while automatically providing optimization strategies for computation. It achieves significant speedups for block copolymers with topological symmetries, and there has been a significant increase in simulation efficiency for the miktoarm polymers and dendrimers, which have aroused general interest in recent theoretical and experimental studies.

GENERAL FORMULATION

First, we provide a brief introduction to the graph representation of arbitrary non-cyclic block copolymers and its algorithmic implementation that was proposed in our previous work.[24] For the general formulation of the SCFT framework, a detailed description is also provided in the reference. Here, we focus on the topology-specific propagator definition. To systematically handle complex architectures, the chain architecture is represented by a simple graph $G = (V, E)$, where V represents a set of vertices ($V = \{1, 2, ...n_v\}$) and E is an edge relation ($E \to \{\{u, v\} | u, v \in V\}$) that is both symmetric ($E(u, v) = E(v, u)$ for $u, v \in V$) and irreflexive ($E(v, v)$ is not allowed for $v \in V$). Bijective mappings are established between the edges and vertices of a graph and the blocks and joints of a block copolymer, respectively, as demonstrated in Fig. 1(a). The incidence function $M(u, v)$ assigns properties such as species, block length, chain contour step size, *etc.* to each edge. Vertices with degree 1 are labeled as leaf vertices, while others are joint vertices. One of the joint vertices is designated as the goal vertex, serving as the terminus of propagator pathways. This designation establishes two propagator classes: forward propagators (propagating from leaf vertices to the goal vertex) and backward propagators (propagating from the goal vertex to leaf vertices).

A modified diffusion equation (MDE) is a partial differential equation in the following form:

$$\frac{\partial q_{uv}(\mathbf{r}, s)}{\partial s} = \nabla q_{uv}(\mathbf{r}, s) - w(\mathbf{r}) q_{uv}(\mathbf{r}, s) \tag{1}$$

where $q_{uv} = q_{uv}(\mathbf{r}, s)$ is a propagator starting from vertex u and ending with vertex v, a function of both position ($\mathbf{r}$) and coordinate along the chain contour (s), and $w(\mathbf{r})$ is the auxiliary field for the specie that can be inferred from $M(u, v)$. In other words, the specie consisting of a polymer block determines which auxiliary field to use in the MDE. The initial condition of an MDE for q_{uv} is $q_{uv}(\mathbf{r}, 0)$, which is the product of propagators coming from all connected blocks at the vertex u, *i.e.* $q_{uv}(\mathbf{r}, 0) = \prod_i q_i(\mathbf{r}, f_i)$, where f_i is the length of the i^{th} block that connects to the current block, as depicted in Fig. 1(b). Note that the initial condition of the MDE starting from a leaf vertex is always $q(\mathbf{r}, 0) = 1$.

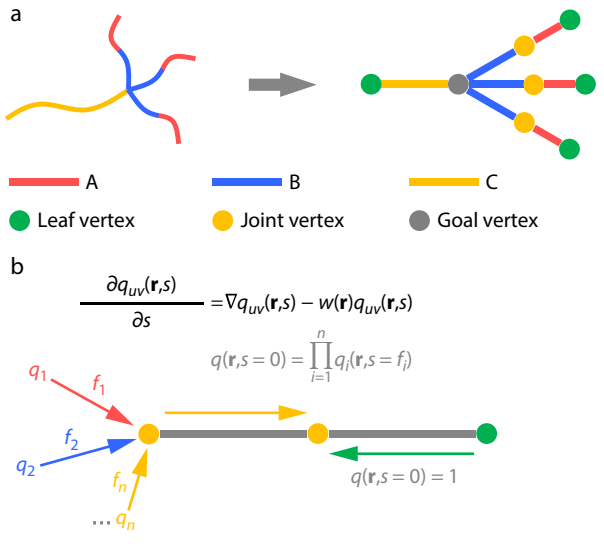

Fig. 1 (a) Schematic diagram of the graph representation of block copolymers. Mappings between edges and vertices of the graph and blocks and joints of the block copolymer, respectively. (b) Propagators and the corresponding modified diffusion equation.

In addition, all spatial lengths are scaled by the radius of gyration of an unperturbed linear chain with N segments, $R_g = \sqrt{Nb^2/6}$ (where b is the statistical segment length), and the chain contour variable s is normalized to the interval [0, 1].

The form of the MDE implies that its solutions are fully determined by the auxiliary field, the domain of s, and the initial condition. Obviously, all these components depend on the specific chain architecture. Thus, as a conventional approach, each chain architecture requires a specific implementation of the SCFT algorithm, which hinders the switch of chain architecture online during an SCFT simulation. In our previous work,[24] we utilized a graph representation to implement a universal SCFT program which can perform simulations for block copolymers with arbitrary non-cyclic chain architectures. Here, we aim to accelerate the graph-enhanced SCFT simulation by further exploring the symmetry of the chain architecture.

We first elucidate the concept of subtrees using the graph representation of the chain architecture shown in Fig. 1(a) as an example. Within our graph representation constructed from non-cyclic block copolymer chains, these tree-like architectures can be progressively decomposed until reaching individual constituent blocks. Structural units larger than single blocks but smaller than the complete molecular chain are defined as subtrees. This decomposition process is illustrated in Fig. 2(a), where the $C(AB)_3$ structure undergoes sequential fragmentation: initially separated into C– and $-(AB)_3$ subtrees, followed by further division of $-(AB)_3$ into -AB subtrees,

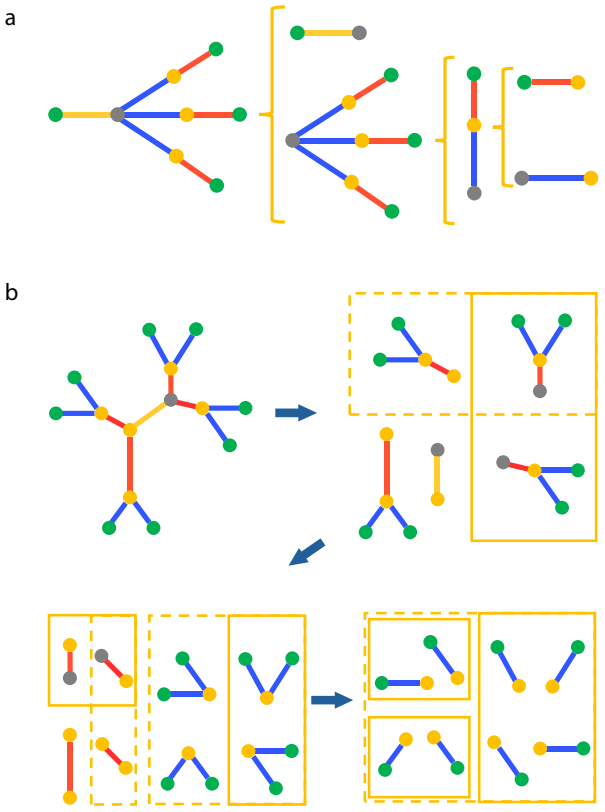

Fig. 2 The decomposition process of block copolymer for subtrees. Dashed-line and solid-line boxes represent semi-equivalent and equivalent relationships, respectively.

ultimately yielding elementary A- and B- blocks. The shared vertex that connects a subtree to its parent architecture is designated as the *front vertex*.

Subsequently, we establish rigorous definitions for *equivalent*, *semi-equivalent* and *non-equivalent* subtrees. Two propagators are considered equivalent if they share the same initial condition and block properties (specie type and block length). Thus, the MDEs associated with them are identical and can be solved only once. Note that one polymer block has two propagators (both forward and backward) associated with them. Two polymer blocks are equivalent if they have two pairs of equivalent propagators, while they are semi-equivalent if they have only one pair of equivalent propagators. Two subtrees are equivalent if they satisfy the following conditions: (1) they are isomorphic, and (2) all blocks in these two subtrees can be pairing as equivalent blocks. Two subtrees are semi-equivalent if the "equivalent blocks" in the second condition changes to "semi-equivalent blocks". Two subtrees are non-equivalent if they are neither equivalent nor semi-equivalent.

Fig. 2(b) demonstrates this hierarchical equivalence analysis through structural decomposition. Starting from the central yellow C block, the architecture is divided into four $-AB_2$ subtrees. Subsequent division of these $-AB_2$ units produces -A segments and B_2 substructures, which ultimately dissolve into eight terminal -B segments. Dashed-line and solid-line boxes are employed to distinguish semi-equivalent and equivalent relationships, respectively. Initial examination reveals that all four $-AB_2$ subtrees exhibit structural isomorphism. However, the lower-left subtree was excluded from comparison because of its elongated A block which violates the equivalence condition. Among the remaining three $-AB_2$ subtrees, pairwise analysis demonstrates semi-equivalence through established bijective correspondence in forward propagator arrangements. Notably, the upper-right pair achieves full equivalence through the shared front vertex. This topological congruence induces identical initial conditions for backward propagation, thereby satisfying both directional equivalence criteria. The differentiation between semi- and full equivalence emerges from this directional sensitivity in propagator matching requirements. For the eight terminal -B blocks, each pair connected to a shared front vertex demonstrates full equivalence, whereas all -B blocks within equivalent $-AB_2$ subtrees maintain full equivalence. The lower left $-B_2$ subtree exhibits semi-equivalence with the remaining three $-B_2$ subtrees. Consequently, while all -B blocks in this molecular architecture demonstrate semi-equivalence at the global level, specific subsets exhibit full equivalence through their shared topological connectivity.

We subsequently propose an algorithm devised to maximize equivalence detection within chain architectures while achieving computational simplification in propagator analysis. For a given polymer architecture, the selection of a specific goal vertex acts as the root, imposing a directionality on all edges such that they point from the peripheral leaf vertices inward toward the goal vertex. Based on this directed representation, a modified breadth first searching (BFS) algorithm is implemented to systematically traverse all polymer blocks, generating propagators with associated traversal levels (de-

https://doi.org/10.1007/s10118-026-3599-4

noted L). The level is defined in such a way that: the level $L = 1$ contains propagators originating from the leaf vertices, initialized with $q(\mathbf{r}, 0) = 1$. The level $L = k$ $(k \geq 2)$ comprises propagators whose computation strictly requires prior results from the propagators in $L = k - 1$. This hierarchical sequencing emerges naturally from the edge directionality in our graph representation, where the traversal propagates from peripheral leaves toward the central goal vertex. The result sequence guarantees that propagator calculations at level $L = k$ are executable only after completing all the propagator calculations at level $L = k - 1$.

When all propagator calculation sequences are obtained, we can reduce the number of MDE solutions required by comparing the subtree equivalence within each traversal level. While the assignment of propagators to specific traversal levels varies with the choice of the goal vertex, the resulting set of independent propagators (equivalence groups) is intrinsic to the chain topology. Since the propagator evolution is strictly anchored by the fixed initial conditions ($q(\mathbf{r}, 0) = 1$) at the leaf vertices, the topological decomposition yields an identical minimal set of required evaluations, derived from identifying both equivalent and semi-equivalent substructures, regardless of which joint vertex serves as the goal. Consequently, the algorithm arbitrarily selects a joint vertex to initiate the decomposition, ensuring minimal MDE computations.

The Algorithm 1 presents a pseudo code that implements the above algorithm, which generates the independent equivalence groups through dependency analysis based on an arbitrarily selected goal vertex.

Algorithm 1: Topological decomposition

input : Polymer graph G, Block properties M
output: Equivalence groups Π

```
Arbitrarily select a vertex r ∈ V with degree(r) > 1;
seq ← Reverse(BFS(G, root = r))          // bottom-up dependency order
Groups ← Φ;
foreach prop p ∈ seq do
    matched ← false;
    foreach g ∈ Groups do
        if IsEquiv (p, g, M, Groups) then
            add p to g; matched ← true; break;
        end
    end
    if not matched then add {p} to Groups;
end
Π ← Groups;
return Π;
```

Beyond defining topological connectivity, this rigorous graph representation inherently supports solver-level optimizations such as propagator aggregation.[26] Distinct from methods relying on manual pre-classification of strand types, our framework offers a fully automated pathway to identify these aggregation candidates within arbitrary topologies, providing a robust basis for propagating single aggregated trajectories in future extensions.

NUMERICAL IMPLEMENTATION

To quantitatively analyze the acceleration efficiency of our algorithm, we introduce two key parameters: the relative time contribution of propagator calculations without considering architecture symmetry (D) and the acceleration factor (A). The parameter D represents the proportion of time spent on propagator calculations relative to the total SCFT calculation time. Typically, D reaches 70% for the OS2 method and exceeds 90% ($D >$ 90%) for the RQM4 method. The theoretical speedup factor (S) can be estimated using the following expression:

$$S = \frac{1}{1 - D + D/A} \tag{2}$$

where $1 - D$ corresponds to the portion of the computation that cannot be accelerated. For individual propagators, the computational time is approximately proportional to the number of chain contour steps of each block. The acceleration factor can then be estimated using the following expression:

$$A = \frac{\sum_{i \in P} f_i / \Delta s_i}{\sum_{i \in P^*} f_i / \Delta s_i} \tag{3}$$

where P and P^* represent the complete set of propagators and the remaining propagators requiring computation after acceleration, respectively. f_i denotes the length of the propagator i and Δs_i is the corresponding contour step size. In the description below, we keep the contour step sizes Δs_i uniform across all blocks, so that the acceleration factor is defined as:

$$A_f = \sum_{i \in P} f_i / \sum_{i \in P^*} f_i \tag{4}$$

In the following Benchmark section we additionally discuss the more fundamental definition of the acceleration factor A built on the number of contour steps, $N_s^i = f_i / \Delta s_i$.

Fig. 3(a) demonstrates the computational optimization achieved according to our proposed algorithm in a complex chain architecture, where the hierarchical subtrees G_1, G_2, and G_3 represent progressively smaller structural units, respectively. Initiating the decomposition from the goal vertex, the molecular structure is divided into two fully equivalent G_1-class subtrees and one G_2-class subtrees that maintains the topological isomorphism with G_1 but lacks equivalence. Further subdivision of the G_2 subtree reveals a pair of equiva-

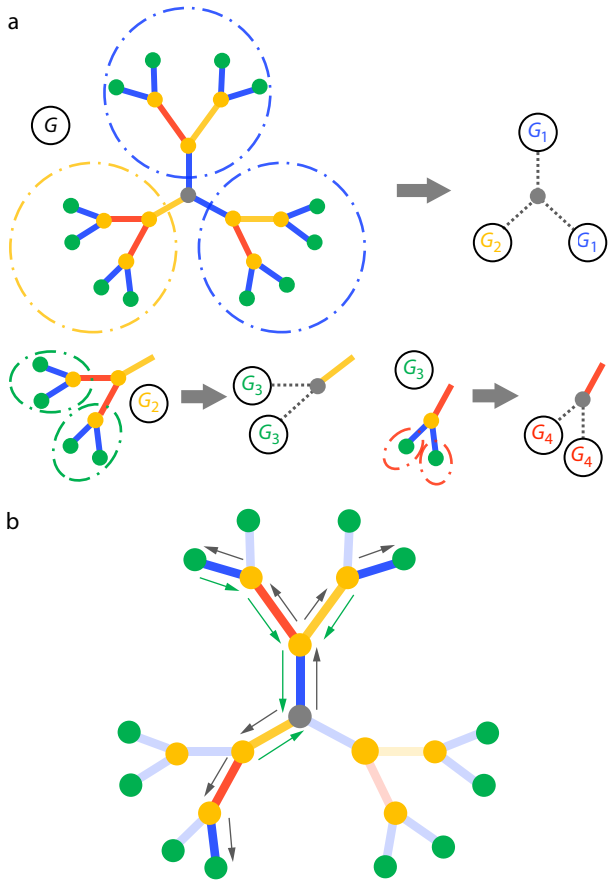

Fig. 3 An example for the computational optimization achieved through our proposed framework in a complex molecular architecture. The blue, yellow, green and red dashed boxes in (a) denote the G_1, G_2, G_3 and G_4 subtrees, respectively. G is the original graph representation. The green and grey arrows in (b) indicate the forward and backward propagators, respectively.

lent -AB_2 subtrees (denoted as G_3 in green dashed boxes), which exhibit semi-equivalence relative to the -AB_2 subtrees embedded within the two G_1-class parent structures. The G_3 subtrees are finally decomposed into G_4, which are also fully equivalent within G_3 and semi-equivalent to the terminal B-blocks in G_1. Fig. 3(b) quantifies gains in computational efficiency through reduction of the number of propagator evaluations. Solid lines indicate essential propagator computations post-optimization, while dashed lines represent the eliminated redundant calculations. The number of propagators to be calculated is reduced from 42 to 13. If we assume all block lengths are equal, then the acceleration factor can be easily computed as $A = 42/13 \approx 3.2$. Consequently, assuming $D = 90\%$ leads to a theoretical speedup about 2.6.

BENCHMARKS

In this benchmark analysis, we selected representative chain topologies that are currently of significant interest in both experimental and theoretical investigations: AB_4 miktoarm star copolymers, $(AB)_5$ multiblock copolymers, and $A(B(B)_2)_3$ dendrimer-like copolymers. The test systems encompassed classical complex ordered phases: A15 phase, σ phase, double gyroid networks, and O^{70} network. Through empirical acceleration measurements, we subsequently reverse-engineered the corresponding D values.

Performance Benchmarks Based on Block Length

We begin by analyzing the speedup predicted by the simplified f_i-based model (Eq. 4), under the assumption of a uniform discretization Δs. Fig. 4 illustrates the broad applicability of our acceleration methodology across challenging combinations of complex molecular topologies and ordered self-assembled phases. Figs. 4(a)–4(c) depict schematic representations of the three polymer architectures considered in this study: AB_4 mik-

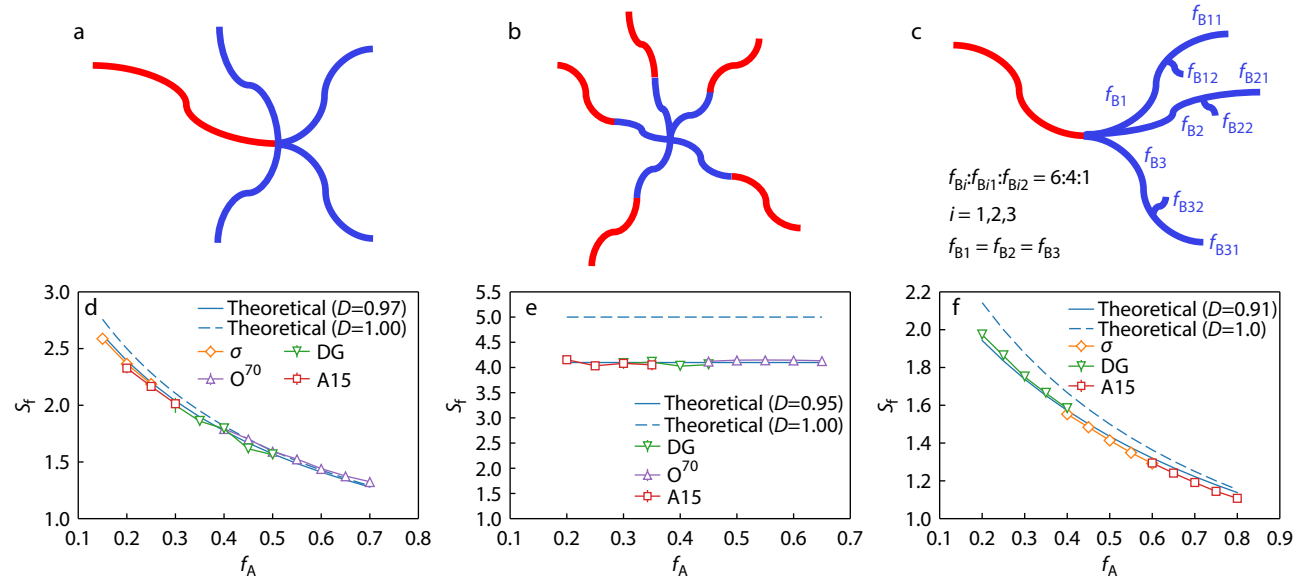

Fig. 4 Schematic representations of the three polymer architectures studied: (a) AB_4 miktoarm star copolymer, (b) (AB_5) linear multiblock copolymer, and (c) asymmetric dendrimer-like structure $A(B(B)_2)_3$. (d–f) Measured speedup S_f as a function of f_A for the corresponding topologies. The dashed line illustrates the theoretical acceleration factor for an assumed proportion D of 1.0, whereas the solid line represents the curve fitted to the actual simulation acceleration data by adjusting D.

https://doi.org/10.1007/s10118-026-3599-4

toarm star copolymers, $(AB)_5$ multiblock copolymers, and asymmetric dendrimer-like molecules $A(B(B)_2)_3$, respectively.

The corresponding measured speedup S_f as a function of the volume fraction f_A is shown in Figs. 4(d)–4(f). For both the AB_4 and $(AB)_5$ architectures, the achievable computational reduction obtained from propagator reutilization exhibits a clear correlation with the lengths of equivalent propagators. As f_A increases, progressive shortening of the B-blocks leads to monotonic degradation in acceleration efficiency A_f, causing a reduction in the observed speedup S_f. To further assess performance in highly asymmetric, branched architectures, we investigated $A(B(B)_2)_3$ dendrimer-like topology, in which a central A block connects to three B branches of equal segment fraction f_{B1}, each subsequently splitting into two unequal terminal B segments (volume fraction ratio 1:4). As shown in Fig. 4(f), the trend in numerical S_f closely follows the theoretical curve, again displaying a decreasing S_f with increasing f_A. These results confirm that the f_i-based model provides a robust and predictive heuristic for estimating acceleration effectiveness, even for asymmetric and highly branched architectures. Notably, RQM4 implementations demonstrated D values in the 91%–97% range across all three systems, indicating that the algorithm effectively targets the dominant computational bottleneck, thus enhancing overall efficiency at its fundamental source.

Discretization-based Acceleration

While the f_A-based analysis is predictive, it relies on the simplifying assumption of a uniform contour step size (Δs) across all blocks. In this scenario, $N_s^i \propto f_i$, where N_s^i is the number of discretization steps for block i. However, the true computational cost of solving the MDE (Eq. 1) is not directly proportional to the block's volume fraction f_i, but rather is strictly proportional to the number of discretization steps N_s^i, required to solve its propagator. This distinction is critical. Adhering to a uniform Δs for architectures with disparate block lengths leads to substantial computational redundancy. To ensure numerical accuracy for short blocks, a small Δs is requisite; however, applying this fine resolution globally results in an excessively large N_s for long blocks, thereby inflating the computational cost without proportional benefits.

To overcome this, a flexible discretization strategy—where N_s^i (or Δs_i) can be set independently for each block—is essential for balancing accuracy and efficiency. A key feature of our graph-enhanced SCFT platform is its native support for this flexible discretization, which enables optimal assignment of N_s values to maintain numerical accuracy while minimizing computational cost. Consequently, we redefine the topological acceleration factor A_N, to reflect the actual computational workload. We reformulate Eq. (3) in terms of the discretization steps $N_s^i = f_i/\Delta s_i$:

$$A_N = \frac{\sum_{i\in P} f_i/\Delta s_i}{\sum_{i\in P'} f_i/\Delta s_i} = \frac{\sum_{i\in P} N_s^i}{\sum_{i\in P'} N_s^i} \tag{5}$$

This N_s-based definition precisely quantifies the computational work saved by the algorithm.

Validation of N_s-Dependent Acceleration

To validate the N_s-based model, we conducted a second series of benchmark tests on the AB_4, $(AB)_5$, and $A(B(B)_2)_3$ architectures, with the volume fractions f_i held fixed for each topology, as shown in Figs. 5(a)–5(c). We varied the number of contour discretization steps in the A-block, N_s^A, and recorded the corresponding acceleration performance. Figs. 5(d)–5(f) present the measured speedup S_N as a function of N_s^A. In all cases, the experimental measurements exhibit strong agreement with the theoretical prediction A_N (dashed curves, evaluated using Eq. (4) assuming $D = 1.0$). These results clearly demonstrate that N_s—rather than f_i is the fundamental determinant of acceleration efficiency. The persistent gap between the measured S_N and the theoretical $D = 1.0$ curve empirically validates our speedup model (Eq. 2), confirming that $D < 1.0$ consistently.

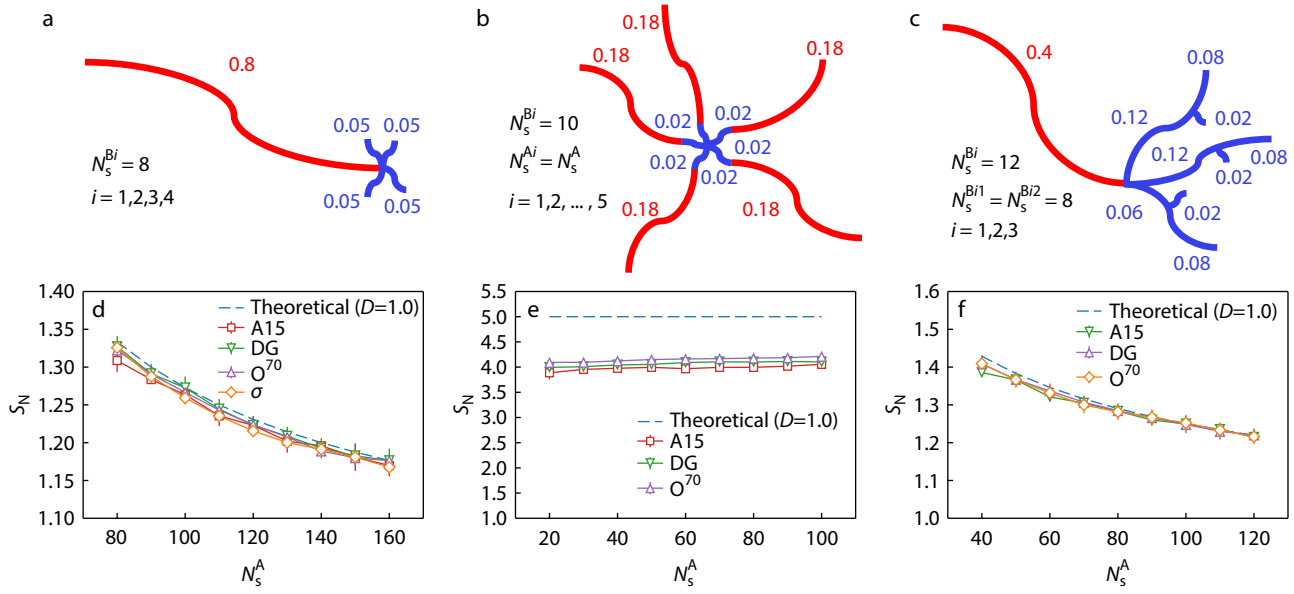

Fig. 5 (a–c) Schematic representations of the polymer architectures evaluated in the N_s-based benchmark: (a) AB_4, (b) $(AB)_5$, and (c) asymmetric dendrimer. (d–f) Measured speedup S_N as a function of the A-block discretization N_s^A for the corresponding systems in (a–c).

https://doi.org/10.1007/s10118-026-3599-4

Table 1 Number of independent propagators to be computed for a single chain across all topologies, with and without acceleration, for given structural parameters m.

Architecture	Non-accelerated	Accelerated	A_m
AB_m	$2 + 2m$	4	$(1 + m)/2$
$(AB)_m$	$4m$	4	m
Dendrimer with depth of m	$3^{m+1} - 3$	$2m$	$(3^{m+1} - 3)/2m$

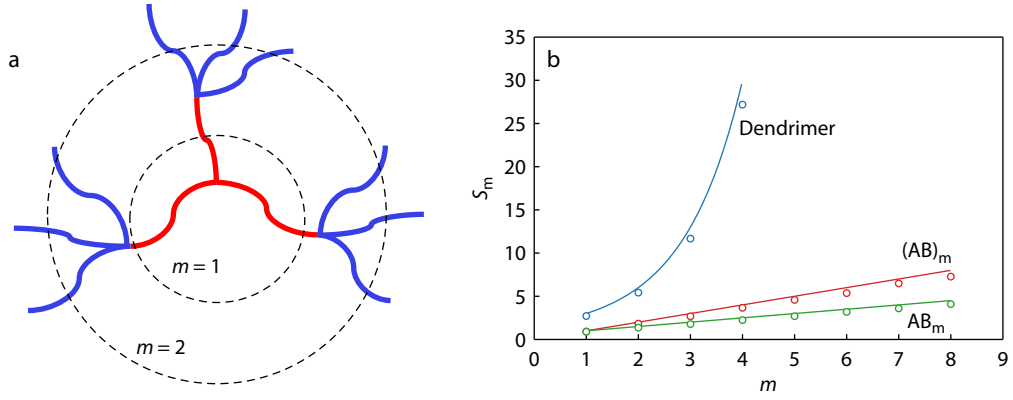

Fig. 6 (a) Dendrimer topology with three child nodes and depth of m where $m = 2$. The m^{th} layer consists of blocks of species B; all remaining layers comprise species A. (b) Measured speedup S_N as a function of the structure parameters m. The solid line represents the theoretical S_m with $D = 1.0$, which corresponds to A_m.

This test also verifies the robustness and general applicability of the acceleration algorithm. In the $A(B(B)_2)_3$ system, we introduced asymmetry by altering the length of one of the three primary B-branches (B3 connected to A), rendering it distinct from the other two (B1 and B2), as shown in Fig. 5(c). Importantly, the algorithm correctly identifies this case as semi-equivalence (as defined in Fig. 2b). While the modification breaks full equivalence among the three branches, the terminal B-blocks attached to them remain semi-equivalent. Consequently, the inward propagators for terminal B-blocks remain equivalent for all three groups. The algorithm detects this partial symmetry, reusing the shared inward propagators and recomputing only the outward propagators and the unique B3 segment. This behavior demonstrates correct symbolic detection of propagator equivalence and validates efficient reuse even in partially symmetric topologies.

Crucially, this capability to independently optimize discretization levels (N_s) distinguishes the present framework from the dynamic programming approach by Yong and Kim.[25] While such method effectively exploits path containment to reuse trajectories, it typically necessitate a uniform contour step size (Δs) across all blocks to ensure grid alignment. In contrast, our strategy prioritizes the flexibility to assign optimal N_s to each block. This design choice proves particularly advantageous for discrete mixtures of highly asymmetric architectures, where preventing the inefficient over-discretization of long blocks outweighs the benefits of path reuse. Future extensions of our framework will aim to incorporate path containment detection logic that, under the condition of a chosen uniform Δs, identifies and reuses propagator trajectories for blocks differing only in physical length.

Performance Benchmarks based on Structure Parameters *m*

We further investigated the influence of the structural parameters m, which controls the specified chain architecture. As summarized in Table 1, we selected the architectures AB_m and $(AB)_m$, which extend the previously discussed AB_4 and $(AB)_5$ structures, as well as the dendrimer architecture studied by Yong and Kim,[25] where each branching node generates three child nodes with a total depth of m, as illustrated in Fig. 6(a). For both the accelerated and non-accelerated simulations, we used a consistent discretization steps N_s. Accordingly, the structural factor A_m is defined as the ratio between the number of independent propagators before and after optimization:

$$A_m = \frac{\sum_{i \in P} N_s}{\sum_{i \in P^*} N_s} = \frac{\text{count}(P)}{\text{count}(P^*)} \tag{6}$$

The variation of S_m with respect to m, as shown in Fig. 6(b), demonstrates that the simulated speedup S_m approaches the theoretical prediction A_m (corresponding to $D = 1.0$). This agreement confirms that the proposed algorithm achieves the expected time-complexity scaling.

CONCLUSIONS

In summary, we present an acceleration framework for graph-enhanced SCFT that enables efficient simulation of arbitrary non-cyclic polymer architectures, addressing the growing computational demands associated with complex chain topologies and mesophase structures. By leveraging topological decomposition and hierarchical subtree analysis, the method systematically identifies and consolidates equivalent propagators, thereby eliminating redundant evaluations of their associated MDEs. Benchmark studies on representative systems, including AB_4 star copolymers, $(AB)_5$ multiblock copolymers, and $A(B(B)_2)_3$ dendrimer-like copolymers, demonstrate substantial computational speedups across both classical (A15, σ) and complex (O^{70}, double gyroid) mesophases. These results underscore the

https://doi.org/10.1007/s10118-026-3599-4

framework's ability to achieve significant acceleration by exploiting chain topology symmetries and reducing propagator computation redundancy.

The graph isomorphism-driven approach offers several key advantages in handling complex polymer architectures. First, it provides a more intuitive and streamlined workflow by directly analyzing the chain's topological structure to identify equivalent subtrees, simplifying the optimization process without requiring abstract encoding or multi-step dependency abstraction. Second, the method systematically processes arbitrary symmetries, extending beyond specific degeneracies to encompass weakly nested or mixed-symmetry structures, such as miktoarm stars with non-uniform arms, ensuring broader applicability. Finally, smooth integration with our prior graph-enhanced SCFT framework enables online architecture switching and accelerated execution across entire simulation pipelines, facilitating automated screening and efficient exploration of vast parameter spaces. As a symmetry-based acceleration strategy rooted in graph theory, the method is inherently complementary to existing approaches such as advanced MDE solvers and iterative convergence schemes, and is readily extensible to broader FBS paradigms. Together, these features offer a robust and scalable computational tool for future studies involving increasingly intricate chain architectures and expanded regions of parameter space.

Conflict of Interests

The authors declare no interest conflict.

Data Availability Statement

The procedures for block copolymer construction and graph-based optimization analysis are implemented through open-source software, with source code available at the following repositories: https://github.com/liuyxpp/Polymer.jl and https://github.com/liuyxpp/PolymerArchitecture.jl. Further inquiries regarding this work can be addressed to the author *via* email at 24210440016@m.fudan.edu.cn upon reasonable request.

ACKNOWLEDGMENTS

This work was supported by the National Natural Science Foundation of China (No. 21873021).

REFERENCES

1 Braga, D.; Grepioni, F. *Crystal engineering: from molecules and crystals to materials*; Springer Netherlands: Dordrecht, **1999**.
2 Glotzer, S. C.; Solomon, M. J. Anisotropy of building blocks and their assembly into complex structures. *Nat. Mater.* **2007**, *6*, 557–562.
3 van Anders, G.; Ahmed, N. K.; Smith, R.; Engel, M.; Glotzer, S. C. Entropically patchy particles: engineering valence through shape entropy. *ACS Nano* **2014**, *8*, 931–940.
4 Dshemuchadse, J. Soft matter crystallography—complex, diverse, and new crystal structures in condensed materials on the mesoscale. *J. Appl. Phys.* **2022**, *131*, 020901.
5 Allmann, R.; Hinek, R. The introduction of structure types into the Inorganic Crystal Structure Database ICSD. *Acta Crystallogr. A* **2007**, *63*, 412–417.
6 Lee, S.; Bluemle, M. J.; Bates, F. S. Discovery of a Frank-Kasper σ phase in sphereforming block copolymer melts. *Science* **2010**, *330*, 349–353.
7 Bates, F. S.; Fredrickson, G. H. Block copolymers–designer soft materials. *Phys. Today* **1999**, *52*, 32–38.
8 Boles, M. A.; Engel, M.; Talapin, D. V. Self-assembly of colloidal nanocrystals: From intricate structures to functional materials. *Chem. Rev.* **2016**, *116*, 11220–11289.

Graphical Abstract

Accelerating Field-based Simulations of Block Copolymers By Exploring Symmetry of Chain Architectures

Jun-Yang Liu, Yu-Chen Zhang, and Yi-Xin Liu

Fudan University

A topology-driven acceleration algorithm leveraging graph isomorphism is introduced for polymer field-based simulations. It systematically eliminates propagator redundancies in arbitrary non-cyclic architectures, serving as a front-end enhancement to various field-based simulation frameworks.

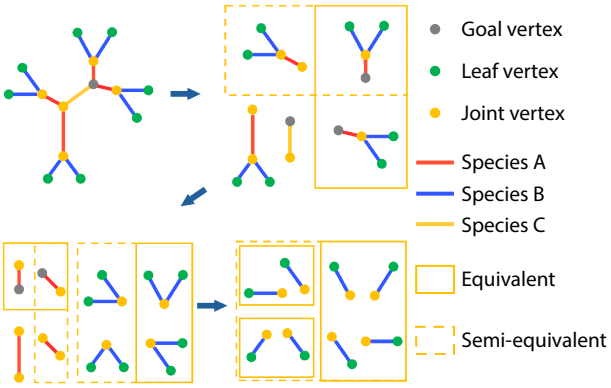

Chinese J. Polym. Sci., 2026 *https://doi.org/10.1007/s10118-026-3599-4*

9 Fredrickson, G. H. *The Equilibrium Theory of Inhomogeneous Polymers*; Oxford University Press, **2005**.
10 Seo, Y.; Woo, D.; Li, L.; Li, W.; Kim, J. K. Phase behavior of PS-(PS-b-P2VP) miktoarm star copolymer. *Macromolecules* **2021**, *54*, 7822−7829.
11 Ma, Z.; Liu, Z.; Zheng, T.; Gan, Z.; Tan, R.; Dong, X. H. Discrete miktoarm star block copolymers with tailored molecular architecture. *ACS Polym. Au* **2023**, *3*, 457−465.
12 Woo, D.; Yoon, H.; Li, L.; Dong, Q.; Li, W.; Kim, J. K. High-density packing of spherical microdomains from A(AB3)3 dendron-like miktoarm star copolymer. *ACS Macro Lett.* **2023**, *13*, 8−13.
13 Hou, W.; Feng, Y.; Zhou, Y.; Yin, X.; Liu, H.; Liu, Z.; Zhao, T.; Shi, Y.; Chen, Y. Rapid and efficient synthesis of star polymers via arm-first monomer emulsified aqueous ring-opening metathesis polymerization (ME-ROMP). *Macromolecules* **2024**, *57*, 3173−3182.
14 Levi, A. E.; Fu, L.; Lequieu, J.; Horne, J. D.; Blankenship, J.; Mukherjee, S.; Zhang, T.; Fredrickson, G. H.; Gutekunst, W. R.; Bates, C. M. Efficient synthesis of asymmetric miktoarm star polymers. *Macromolecules* **2020**, *53*, 702−710.
15 Xu, Z.; Dong, Q.; Li, W. Architectural design of block copolymers. *Macromolecules* **2024**, *57*, 1869−1884.
16 Hamley, I. W. in *Developments in block copolymer science and technology*, J. Wiley, **2004**.
17 Spencer, R. K. W.; Matsen, M. W. Field-theoretic simulations of bottlebrush copolymers. *J. Chem. Phys.* **2018**, *149*, 184901.
18 Gompper, G.; Schick, M. in *Soft matter. Vol. 1 Polymer melts and mixtures*, Wiley-Vch, **2006**.
19 Rasmussen, K. O.; Kalosakas, G. Improved numerical algorithm for exploring block copolymer mesophases. *J. Polym. Sci. B* **2002**, *40*, 1777−1783.
20 Ranjan, A.; Qin, J.; Morse, D. C. Linear response and stability of ordered phases of block copolymer melts. *Macromolecules* **2008**, *41*, 942−954.
21 Song, J.-Q.; Liu, Y.; Zhang, H. An efficient algorithm for self-consistent field theory calculations of complex self-assembled structures of block copolymer melts. *Chinese J. Polym. Sci.* **2017**, *36*, 488−496.
22 Qiang, Y.; Li, W. Accelerated pseudo-spectral method of self-consistent field theory via crystallographic fast fourier transform. *Macromolecules* **2020**, *53*, 9943−9952.
23 Arora, A.; Morse, D. C.; Bates, F. S.; Dorfman, K. D. Accelerating self-consistent field theory of block polymers in a variable unit cell. *J. Chem. Phys.* **2017**, *146*, 244902.
24 Zhang, Y.; Huang, W.; Liu, Y. X. Automated chain architecture screening for discovery of block copolymer assembly with graph enhanced self-consistent field theory. *Commun. Mater.* **2024**, *5*, 266.
25 Yong, D.; Kim, J. U. Dynamic programming for chain propagator computation of branched block copolymers in polymer field theory simulations. *J. Chem. Theory Comput.* **2025**, *21*, 3676−3690.
26 Li, C.; Delaney, K. T.; Shell, M. S.; Fredrickson, G. H. Efficient computation of single-chain partition functions in field-theoretic simulations of polymers with nested tree-like topologies. *Macromol. Theor. Simul.* **2025**, *34*, e70000.

https://doi.org/10.1007/s10118-026-3599-4